scientific reports

Check for updates

OPEN

The synergistic anti-leishmanial effect of photodynamic therapy employing chemotherapy-mediated nanocomposites

Elahe Molaakbari[1], Ahmad Khosravi[1]✉, Ehsan Salarkia[1], Iraj Sharifi[1], Alireza Keyhani[1], Mehdi Bamorovat[1], Mohammad Zarif[1] & Fatemeh Sharifi[2]

Cutaneous leishmaniasis (CL) presents a significant therapeutic challenge due to limitations of current treatments like meglumine antimoniate (MAT), including drug resistance and adverse side effects. Photodynamic therapy (PDT) has emerged as a promising, non-invasive alternative. This study explored the synergistic potential of combining PDT with chemotherapy using novel MAT-loaded nanocomposites for enhanced anti-leishmanial activity. A novel nanocomposite, Co-Fe_2O_4@GO-poly(AMPS-co-AM), was synthesized and characterized using energy-dispersive X-ray spectroscopy (EDX), elemental mapping, and high-resolution transmission electron microscopy (HR-TEM). MAT was immobilized onto the nanocomposite, forming NCMAT. The in vitro anti-leishmanial efficacy of NCMAT against L. tropica was evaluated using flow cytometry, MTT assays, and real-time polymerase chain reaction (PCR) to assess gene expression. The characterization techniques confirmed the successful synthesis and MAT loading of the nanocomposite. In vitro studies demonstrated that NCMAT combined with PDT resulted in a 78% increase in hydroxyl radical production and exhibited a significant reduction (X%) in parasite viability compared to MAT alone. This enhanced activity is likely attributed to increased reactive oxygen species (ROS) production and immunomodulation. Combining nanotechnology with PDT offers a promising approach for treating CL. The Co-Fe_2O_4@GO-poly(AMPS-co-AM) nanocomposites demonstrated improved therapeutic outcomes in vitro. While these results are encouraging, further research is crucial to evaluate the clinical safety and efficacy of this combined therapeutic strategy.

Keywords *Leishmania tropica*, Meglumine antimoniate, Amphotricine B, Photosentesizer Co-Fe_2O_4@GO-poly (AMPS-co-AM) nanocomposite, Photodynamic therapy

Leishmaniasis is a neglected vector-borne disease caused by protozoan parasites from *Leishmania.* According to the World Health Organization (WHO), nearly 100 countries with 350 million people are at risk of infection globally. Current estimates indicate between 700,000 and 1 million new cases annually c. Visceral leishmaniasis (VL), cutaneous leishmaniasis (CL), and mucocutaneous leishmaniasis (MCL) are the 3 main types of the disease[1].

CL is the most common type of disease, which is characterized by skin lesions, and most cases occur in eight countries: Afghanistan, Algeria, Brazil, Iran, Pakistan, Peru, Saudi Arabia, and Syria[2]. There are two prevalent forms of CL: anthroponotic cutaneous leishmaniasis (ACL) and zoonotic cutaneous leishmaniasis (ZCL). The ACL form is caused by *Leishmania tropica* (*L. tropica*), a dry or urban type of leishmaniasis[1,3]. Chemotherapy, curettage, and cryotherapy are the standard treatment modalities for CL[4].

Meglumine antimoniate (MA), an antimonial compound with the chemical formula $C_7H_{18}NO_8Sb$, is the primary treatment option for leishmaniasis. Unfortunately, the reported cure rates for antimonial therapies range from 40–70%[5]. The use of antimonial compounds is limited by side effects, such as the painful nature of IL injections and complications like pancreatitis, hepatotoxicity, and cardiac dysfunction associated with systemic injections[6–8]. Second-line drugs such as AMB, liposomal AMB, pentamidine, miltefosine, and paromomycin are often expensive and associated with high toxicity and many adverse effects[9–12]. Additionally, no human vaccine is available yet[13]. Lack of human vaccines, prolonged treatment duration, rapid emergence of drug resistance,

[1]Leishmaniasis Research Center, Kerman University of Medical Sciences, Kerman, Iran. [2]Research Center of Tropical and Infectious Diseases, Kerman University of Medical Sciences, Kerman, Iran. ✉email: khosraviam@yahoo.com

and adverse effects highlight the need for alternative CL therapies[14–16]. To combat increasing drug unresponsive in common treatments, new and complementary treatment methods are needed[17,18].

Photodynamic therapy (PDT) is a promising treatment for diseases such as CL[19,20]. It's non-invasive, minimally damaging, and can be repeated. PDT works by using light to activate a light-sensitive drug, which then generates reactive oxygen species (ROS) that eliminate the causative agent of the disease. Specifically, PDT involves the administration of a photosensitizer, a molecule that is selectively retained in target tissues. Upon irradiation with light of a specific wavelength, the photosensitizer absorbs energy and transfers it to molecular oxygen, leading to the formation of highly reactive species like singlet oxygen and hydroxyl radicals. These ROS cause oxidative stress and damage to essential cellular components, including lipids, proteins, and DNA, ultimately leading to cell death in the targeted cells or pathogens. This approach offers several advantages, including the potential to reduce side effects and improve patient outcomes[21–23].

Light-emitting diodes (LEDs) are semiconductor devices that emit light spontaneously, resulting in a broad spectrum and lower power output compared to diode lasers. This makes them suitable for PDT in resource-limited settings[24]. When choosing a light source for PDT, factors such as treatment area size, disease type, photosensitizer characteristics, and cost should be considered[25].

Non-degradable nanoparticles release reactive oxygen species continuously until cell destruction, while degradable nanoparticles release the photosensitizer gradually. Nanoparticles can enhance PDT by converting light or acting as photosensitizers themselves[26]. They can also aid drug delivery by entering cells and being stored in lysosome-like structures. Magnetic nanoparticles, with their high surface-to-volume ratios and superparamagnetic properties, are particularly useful for drug delivery and separation[27].

Co-Fe_2O_4 spinel ferrite nanoparticles are of great interest due to their unique electrical and magnetic properties and physical and chemical stability. These cobalt ferrite-based nanoparticles are used in various applications, including magnetic recording, lasers, and targeted drug delivery. The degree of inversion in cobalt ferrite's spinel structure varies depending on how it is prepared. The general formula of the cobalt spinel structure is $M_8Fe_{16}O_{32}$, which is composed of eight MFe_2O_4 formula units. Oxygen ions form the spinel framework. M and Fe cations are arranged interstitially in two tetrahedral sub-lattices within the face-centered cubic 1 (FCC 1) network that oxygen ions create in this structure[28,29].

In this study, we utilized a Co-Fe_2O_4@GO-poly(AMPS-co-AM) nanocomposite as our drug delivery platform. This specific formulation was chosen for several key reasons: First, the Co-Fe_2O_4 spinel ferrite nanoparticles offer significant advantages due to their unique magnetic properties, which can be exploited for targeted drug delivery and potential hyperthermia applications[27,30,31]. Second, the graphene oxide (GO) component provides a large surface area for efficient drug loading of both MAT and AMB, and GO can be further modified to enhance its biocompatibility[32,33]. Finally, the poly(AMPS-co-AM) polymer coating on the GO improves the overall stability and biocompatibility of the nanocomposite in biological systems, reducing potential toxicity and aggregation[33–35]. The combination of these components creates a multifunctional nanocomposite with enhanced therapeutic potential.

Multifunctional hybrid nanoparticles have gained significant attention due to their large surface area, ability to carry diverse drugs, and potential for advanced drug delivery. By modifying graphene oxide (GO) with hydrophilic polymers, researchers aim to enhance its solubility, drug-carrying capacity, and biocompatibility. This approach addresses the potential hazards of unmodified GO, making it a more effective drug carrier[30,31].

In addition, applying graphene oxide-containing hybrid biocompatible polymers has shown better drug delivery results in toxicity trials[36–38]. In a recent study by Boroujeni and coworkers[39], GO and Poly (2-acrylamido-2-methyl-1-propanesulfonic acid-co-acrylamide) Grafted on Graphene Oxide (GO-poly (AMPS-co-AM)) fluorescence emission bands were examined under various excitation wavelengths. The researchers found that 360, 400, and 440 nm excitation wavelengths caused fluorescence emission bands at 722, 800, and 880 nm, respectively, related to GO-poly (AMPS-co-AM). This indicates that the GO-poly (AMPS-co-AM) component can be excited by 400 nm light and this informed our choice of LED wavelength[39]. The fluorescence peak intensity of GO-poly (AMPS-co-AM) was improved compared to that of GO due to the presence of C=O and SO_3H groups in poly (AMPS-co-AM) after grafting onto GO. Compounds that exhibit intense fluorescence emission bands have been widely used in various fields, including fluorescent biosensors, in vivo fluorescence imaging, and bimodal photodynamic and photothermal destruction of tumors[32,33].

This study aimed to investigate the potential of Co-Fe2O4@GO-poly (AMPS-co-AM) nanocomposites as an innovative and effective platform for enhancing the drug delivery of two specific compounds, MAT and AMB. Additionally, the research explored the application of these nanocomposites in photodynamic therapy targeting *Leishmania tropica*, the causative agent of ACL. By integrating the unique properties of cobalt ferrite and graphene oxide within a polymer matrix, we anticipated that these nanocomposites would improve the therapeutic agents' stability, efficacy, and controlled release, thereby enhancing the overall treatment outcomes against this infectious disease.

Materials and methods

Synthesis of Co-Fe_2O_4 magnetic nanoparticles

Spinel cobalt ferrite was synthesized using the hydrothermal technique[34,35]. After dissolving $FeCl_3$ and $Co(NO_3)_2{\cdot}6H_2O$ in 20 ml of distilled water in a mole ratio of 2:1, the mixture was vigorously agitated for 30 min at room temperature using a magnetic stirrer at 500 rpm. The NaOH solution (1 M) was added drop by drop while the mixture was stirred for 6 h to achieve pH 11. The next step was to transfer the mixture to an autoclave lined with Teflon and to heat it to 180 °C for 12 h. After being subjected to an external magnetic field for multiple washes with distilled water and ethanol, the precipitate was allowed to dry at 80 °C for 6 h in an oven.

Synthesis of GO–poly (AMPS–co–AM)

The GO-poly(AMPS-co-AM) nanocomposite was prepared by direct synthesis[39]. This way, graphene oxide, AM, and AMPS monomers were mixed simultaneously at a molar ratio of 1:3:3 in 50 ml of ethanol. The corresponding mixture was swirled for 24 h at 65 °C with reflux and N2 gas flow under continuous stirring at 400 rpm. After that, an ultrasonic wave was applied to the ethanolic GO solution (1 g in 50 ml) for an hour. The dispersed GO solution was then combined with AM (1.065 g) and AMPS (1.038 g) monomers, as well as BPO initiator (0.051 g), and the combination was stirred for 24 h under reflux conditions at 400 rpm.

Synthesis of Co-Fe_2O_4@GO–poly (AMPS–co–AM)

Co-Fe_2O_4 nanoparticles coated with ethylene glycol were dispersed in ethanol and subjected to an ultrasound wave for 30 min. Then, GO-poly (AMPS-co-AM) nanocomposite was slowly added to the colloidal solution and stirred at room temperature for 12 h to complete the reaction. The obtained product was washed several times with a mixture of ethanol and water using the magnetic separation method.

Loading of MAT and AMB on the surface of the nanocomposite

The 0.1 gr/ml of Co-Fe_2O_4@GO-poly (AMPS-co-AM) nanocomposites suspension was mixed with 0.15 g/ml MAT or AMB solutions and kept in contact for half an hour to allow for proper binding of the drugs to the nanocomposites. The nanocomposites were then separated from the solution using a magnet. These separations were critical to measuring the amounts of free drugs in the solutions accurately. The absorbances of the separated solutions were measured using a UV spectrophotometer to determine the amounts of free drugs present. The concentration of the drugs on the nanocomposites was then calculated indirectly based on the measured absorbances of the free drugs. Finally, it was determined that 0.196 g of MAT and 0.187 g of AMB were loaded per gram of nanocomposites.

Surface modification of the NCMAT and NCAMB with PEG

The surface of the nanocomposite was modified with PEG to improve biocompatibility and increase its stability in biological systems. A suspension of 0.01 g/ml of the NCMAT or NCAMB was added to 0.01 g/l of PEG solution, and the mixture was stirred for 2 h. Finally, the mixture was dried at 90 °C to complete the modification process.

Light source

A specialized LED device was utilized to excite a solution for the experiment. The device had a power output of 83 mW and was designed to operate at a wavelength of 400 nm, which corresponded to its maximum optical absorption. Our team developed and manufactured the LED device explicitly for this purpose. The in vivo experiment involved applying an energy level of 50.99 J over a light focus area of 4 cm2, which covered the entire distance of 15 cm from the base. This resulted in an energy density of 12.74 J/cm^2[40] The 400 nm wavelength was selected because it aligns with the reported fluorescence excitation peak of the GO-poly(AMPS-co-AM) component of the nanocomposite.

Indirect detection of singlet oxygens and hydroxyl radical

Anthracene was used to identify singlet oxygens and indirectly measure the cellular toxicity caused by the nanocomposites. By studying the absorption spectrum of anthracene, it is possible to indirectly prove the production of singlet oxygen so that the higher the amount of singlet oxygen produced, the more amount of anthracene is converted to anthraquinone and the intensity of absorption or emission of anthracene will decrease[41] First, using ultrasonic waves, 0.01 g of anthracene was dissolved in 10 ml of ethanol. Then, 0.15 ml of the obtained solution was diluted with 1.5 ml of ethanol and added to the nanocomposite solution. Then, its absorption spectrum before and after irradiation for a certain period using the LED for 30 min was analyzed and compared.

Also, Methylene blue was used to identify the hydroxyl radical and indirectly measure another type of cell toxicity caused by the nanocomposites[42,43] For this purpose, 0.001 g of methylene blue was dissolved in 50 ml water. Then, 2 ml of the 0.005 g/l of methylene blue solution was added to 2 ml of 0.001 g/l of the nanocomposite solution. Furthermore, the absorption spectrum before and after irradiation by the LED for a specified period of 30 min was investigated and compared.

Anthracene was used to identify singlet oxygens and indirectly measure the cellular toxicity caused by the nanocomposites. By studying the absorption spectrum of anthracene, it is possible to indirectly prove the production of singlet oxygen so that the higher the amount of singlet oxygen produced, the more amount of anthracene is converted to anthraquinone and the intensity of absorption or emission of anthracene will decrease. 41 First, using ultrasonic waves, 0.01 g of anthracene was dissolved in 10 ml of ethanol. Then, 0.15 ml of the obtained solution was diluted with 1.5 ml of ethanol and added to the nanocomposite solution. Then, its absorption spectrum before and after irradiation for a certain period using the LED for 30 min was analyzed and compared.

Also, Methylene blue was used to identify the hydroxyl radical and indirectly measure another type of cell toxicity caused by the nanocomposites. 42,43 For this purpose, 0.001 g of methylene blue was dissolved in 50 ml water. Then, 2 ml of the 0.005 g/l of methylene blue solution was added to 2 ml of 0.001 g/l of the nanocomposite solution. Furthermore, the absorption spectrum before and after irradiation by the LED for a specified period of 30 min was investigated and compared.

Parasites and cell culture

The promastigote stage of *L. tropica* national standard isolate (MRHO/IR/75/ER) was maintained from Afzalipour Medical School, Kerman, Iran at 25 °C in RPMI1640 accompanied with 10% FBS, and 1% penicillin plus streptomycin. A monocyte human cell line (THP-1) was provided by the Kerman Leishmaniasis Research Center and cultivated in DMEM supplemented with 10% FBS and 0.5% antibiotics (Sigma, Poole, UK) at 37 °C with 5% CO_2 concentration. The differentiation of human THP-1 monocytes into macrophage-like cells (MLC) was induced by phorbol 12-myristate-13-acetate (PMA).

Anti-promastigote assessment

Drug susceptibility assays were performed using exponential phase promastigotes. 90 µl of cultivated promastigotes of *L. tropica* (10^6 cells/ml) was added to a 96-well microtiter plate. Then, as mentioned previously, 10 µl of predetermined MAT, AMB, NCMAT, and NCAMB with and without light were added to individual wells and incubated at 25 °C for 72 h. For the light-only control group, 10 µl of the culture medium (without any drug) was added to the wells, and the promastigotes were exposed to the 400 nm LED light under the same conditions as the treated groups. The termination of reactions, an enzyme-linked immunoabsorbent assay (ELISA) reading assessments, and calculation of the IC_{50} (half maximal inhibitory) were conducted as described elsewhere[44].

Anti-amastigote assessment

To estimate the leishmanicidal activity against *L. tropica* intra-macrophage amastigotes, 200 µl of MLC with 10^7 cells were cultivated for 24 h. Then 200 µl of metacyclic promastigotes were relocated beside parasites and, subsequently, fixed with methanol and Giemsa stained. The minimum concentration of a substance at which 50% of leishmanial organisms are inhibited (IC_{50}) was obtained from the MLC (10:1 ratio). After 24 h, 40 µl of all MAT, AMB, NCMAT, and NCAMB concentrations with and without light were transferred to cells and maintained for 72 h. Cells were flowed over with 50 µl PBS to eliminate free by visualizing Leishman bodies (amastigotes) in 100 MLC under an ophthalmic microscope. After entering the inhibition percentages of the amastigotes, CompuSyn software (version 1.0) was used to draw the CI diagram.

Cytotoxic assessment

The MLC (5×10^5) was seeded at a prearranged density of the examined medicines in 96-well ELISA microplates at 37 °C for 72 h in 5% CO2 pressure to investigate the toxic effect of MAT, AMB, NCMAT, and NCAMB with and without light performing MTT assay. The remaining experimental procedures followed the same procedures as mentioned before. Lastly, the colorimetric MTT proliferation assay was employed to measure cell mortality. The data were stated as the proportion of nonviable cells in culture media treated with MAT, AMB, NCMAT, and NCAMB with and without light relative to the untreated control MLC.

M1 and M2 type cytokines

The quantified expressions of selected T-helper 1 (Th1) and T-helper 2 (Th2) cytokines were identified employing quantitative real-time PCR (qRT-PCR) test on MLC. The entire RNA samples were isolated utilizing the High Pure RNA Isolation Kit (Roche, Basel, Switzerland). Initially, the RNA concentration was determined by Thermo Fisher Scientific nanodrop, and then cDNA was synthesized by Roche Synthesis Kit. The remaining qRT-PCR processes were carried out based on the protocol reported elsewhere[30] In Table 1, the primer's pattern and control gene sequences are presented. Based on the previous report, the full study procedure was carried out[30] The following equivalence was employed to analyze CT: [ΔCT = CT (target) − CT (reference)]. Moreover, the fold change was considered using the relative threshold approach (ΔΔCT).

Template	Forward and reverse sequences (5′–3′)		Product size (bp)
TNF-α	Forward	CAGGCGGTGCCTATGTCTC	161
	Reverse	CGATCACCCCGAAGTTCAGTAG	
IFN-γ	Forward	5-GCCGATGATCTCTCTCAAGTGAT-3	106
	Reverse	5-ACAGCAAGGCGAAAAAGGATG-3	
IL-12	Forward	TGGTTTGCCATCGTTTTGCTG	171
	Reverse	ACAGGTGAGGTTCACTGTTTCT	
IL-10	Forward	CTTACTGACTGGCATGAGGATCA	134
	Reverse	GCAGCTCTAGGAGCATGTGC	
TGF-β	Forward	CCACCTGCAAGACCATCGAC	112
	Reverse	CTGGCGAGCCTTAGTTTGGAC	
iNOS	Forward	ACATCGACCCGTCCACAGTAT	89
	Reverse	CAGAGGGGTAGGCTTGTCTC	
GAPDH	Forward	5-AGGTCGGTGTGAACGGATTTG-3	95
	Reverse	5-GGGGTCGTTGATGGCAACA-3	

Table 1. The detailed primers and locus gene sequences.

Apoptotic profile

Apoptosis of promastigotes was studied by well-designed flow cytometry through the BD Annexin V/ PE Apoptosis Detection Kit- Fisher Scientific. Twelve-well plates of promastigotes (10^6) were used to treat them with sequential concentrations of MAT, AMB, NCMAT, and NCAMB with and without light. Promastigotes were stored at 25 °C for 72 h. Hereafter, the parasite was washed with PBS before being incubated for 15 min at 25 °C in the dark with a ratio of 5: l PE-Annexin-V and 7 l of 7-AAD. Lastly, the proportion of the apoptotic parasites was evaluated using Flowjo software (Version 10.0).

Cell cycle assay

The amastigotes were exposed to varying concentrations of MAT, AMB, NCMAT, and NCAMB with and without light to examine the cell cycle in intra-macrophage amastigotes. They were then incubated at 25 ± 1 °C for 72 h. Subsequently, specific samples were transferred to 1.5 ml of PBS, fixed with methanol, resuspended in 50 µl of RNase (1 mg/ml), and left at room temperature for 30 min. Following this, 1 ml of propidium iodide was added at a 0.1 mg/ml concentration. The DNA content was analyzed using flow cytometry (Becton Dickinson), and the Cell Quest package (BD, USA version 3.3) was used to determine the proportion of parasites in different stages.

ROS production

To measure the average quantity of *L. major* intra-macrophage amastigotes ROS, 10^6 macrophages were treated with IC50 concentrations of MAT, AMB, NCMAT, and NCAMB. Following 24, 48, and 72 h, the cells were loaded with 10 M of a permeate probe diacetate 2′0.7′-dichlorofluorescein (Sigma) diluted in DMSO and incubated at 37 °C for 25 min in 5% atmospheric CO_2. The cells were then rinsed with PBS (pH 7.3). The Marshall Scientific BD Bioscience FacsCanto II Flow Cytometer was used to control ROS and data analyzed by Flowjo software (Version 10.0).

Statistical analyses

All data were studied by SPSS Ver 22.00 (Chicago, IL, USA) accompanied by GraphPad Prism version 8.0 (CA, USA). One-way ANOVA and a Student t-test were used to perceive any significant association among treatment groups at a $P < 0.05$ considerable level. The SPSS probit test was used to get the IC_{50} values. The t-test determined the differences between the IC50 in promastigotes and intracellular amastigotes. The selectivity index (SI) is a measure of toxicity added to the following equation: human macrophages (THP-1) were non-toxic when $CC_{50}/IC_{50} \geq 1$.

Results

Characterized of nanocomposites

Figure 1 provides the nanocomposite analysis through energy-dispersive X-ray spectroscopy (EDX) and corresponding elemental mappings. Figure 1a shows that the nanocomposite contains C, O, S, Fe, and Co elements without impurities. The weight and atomic percentages of these elements is included in Fig. 1a. Figure 1b–f also display the distribution of C, O, S, Fe, and Co elements for the nanocomposite, respectively. In Fig. 2a, HR-TEM images of the nanocomposite are presented at the scales of 10, 50 nm, and 200 nm. The images show semi-spherical morphology and the core and subsequent layers were created. Also, in Fig. 2b, the histogram of the nanocomposites indicates that most of the particle sizes of the nanocomposite are below 50 nm.

Beyond morphology and elemental composition, the colloidal stability of the nanocomposites is crucial for their application. Potential aggregation was addressed through surface modification with PEG, as described in the methods. To assess the effectiveness of this modification, the stability and size distribution of the PEGylated

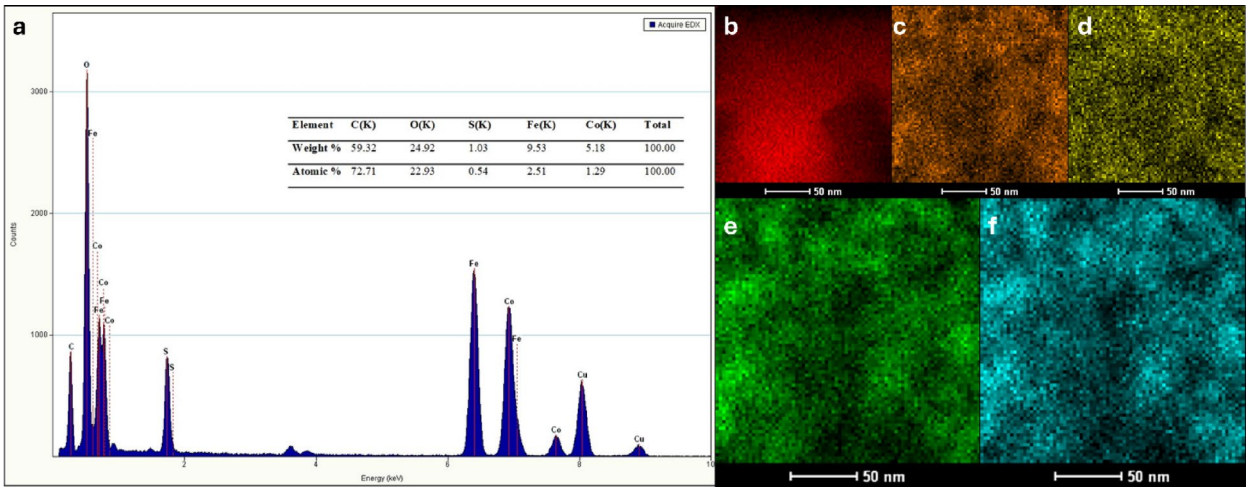

Fig. 1. (**a**) EDX spectrum, (**b**) C element mapping, (**c**) O element mapping, (**d**) S element mapping, (**e**) Fe element mapping, (**f**) Co element mapping and the corresponding mapping distribution of all elementals of the nanocomposites.

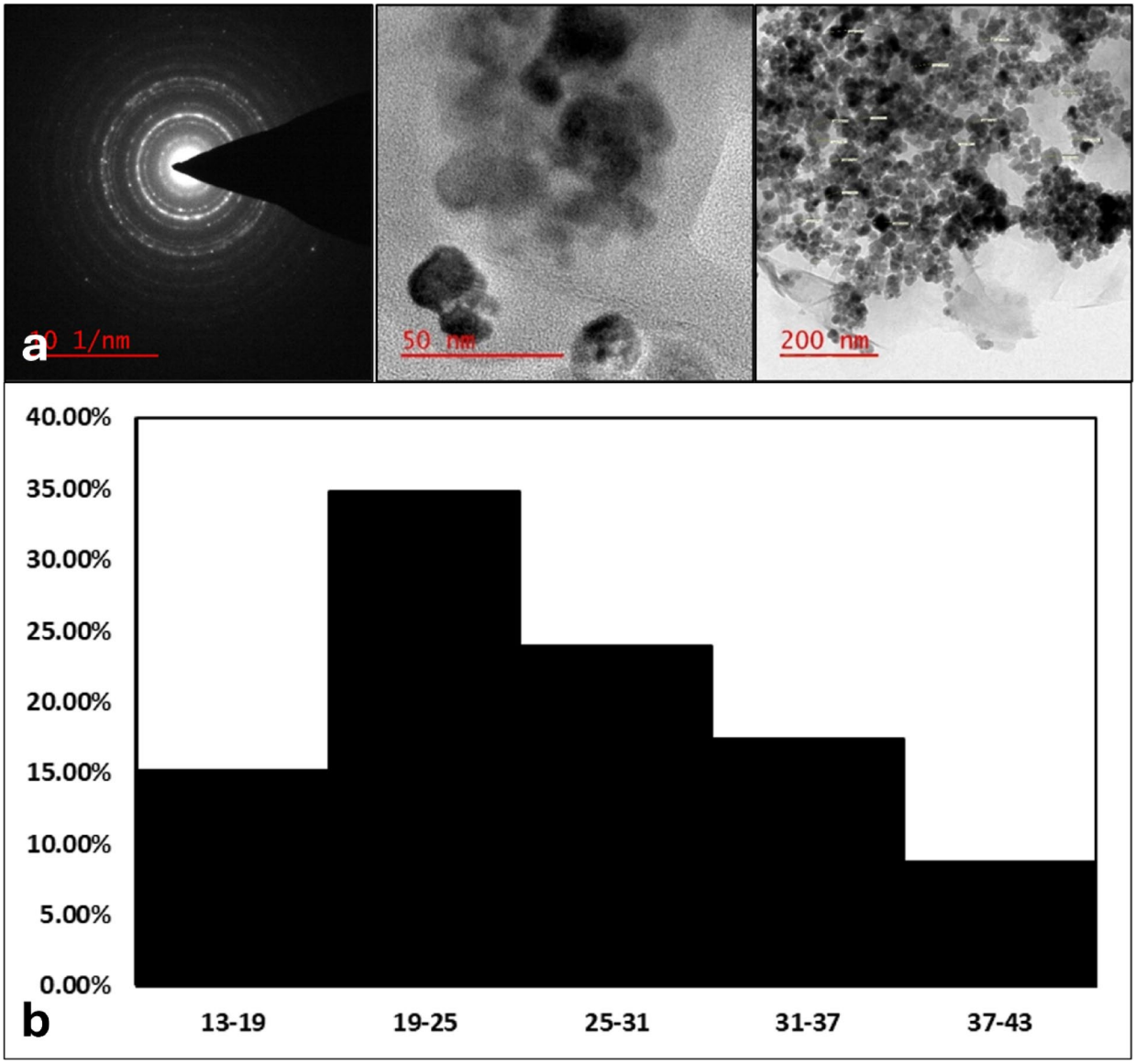

Fig. 2. (**a**) HR-TEM images and (**b**) the histogram of distribution particle size of the nanocomposites.

nanocomposites (NCMAT and NCAMB after PEGylation) in aqueous solution were evaluated over time using Dynamic Light Scattering (DLS). The DLS measurements indicated that PEGylation significantly improved colloidal stability, reducing the tendency for aggregation compared to non-PEGylated counterparts.

Determining the amount of singlet oxygen and hydroxyl radical of nanocomposites in PDT

Figure 3a absorption spectra before (line) and after (dashed line) radiation with LED with 400 nm wavelength radiation can be seen. With singlet oxygen production, anthracene's absorption and emission spectrum should decrease, but the opposite of the increase in intensity is observed in this form. For further investigations, the absorption spectrum was recorded before and after the irradiation of anthracene solution alone for 30 min in the presence of nanocomposite. As seen in Fig. 3a, the absorption intensity of this solution also increased after irradiation.

The results of the experiments show that this material has good optical stability against LEDs with 400 nm wavelength. In this study, the methylene blue solution alone was also examined as the absorption spectrum before and after irradiation[45] (Fig. 3b) for determining the amount of hydroxyl radical in the presence of nanocomposite. This decrease is related to methylene blue solution and should be considered. To compare with the results obtained from reducing the absorption intensity of anthracene, measuring the absorption spectrum of methylene blue with the LED radiation was suggested.

The study found that with the increase of time from 15 min to 60 min, there was no change in the formation of hydroxyl radicals by nanocomposite. As a result, maximum hydroxyl radicals are formed in up to 15 min. However, to ensure the formation of hydroxyl radicals, 30 min was chosen. As it is clear from the data in Table 2, nanoparticles significantly increase the production of hydroxyl radicals. It can be concluded that these

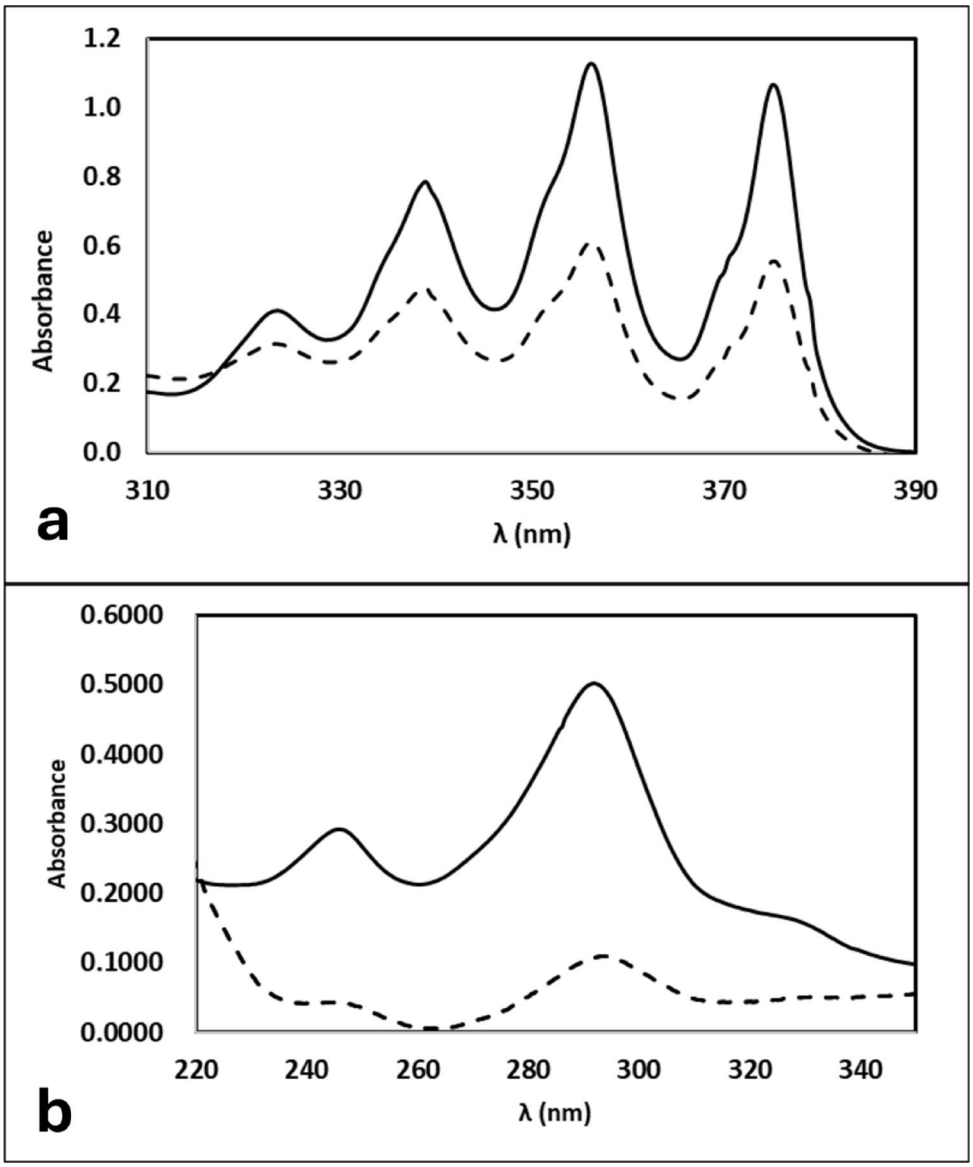

Fig. 3. An anthracene absorption spectrum, before (line) and after (dashed line) irradiation with LED with 400 nm wavelength radiation in the presence of nanocomposite. B Methylene blue absorption spectrum, before and after irradiation with LED with 400 nm wavelength in the presence of nanocomposite.

Analysis	Absorption before irradiation	Absorption after irradiation	% production
Methylene blue	0.5007	0.1046	78.23
Anthracene	1.1205	0.6062	45.90

Table 2. The amount of singlet oxygen and hydroxyl radical in PDT.

nanoparticles have been able to cause and even increase the production of hydroxyl radicals and are helpful in PDT.

Anti-promastigote assessment

The average viability rate of promastigotes at prearranged concentrations of MAT, AMB, NCMAT, and NCAMB with and without light are shown in Fig. 4. All treatment modalities showed significant anti-leishmanial activity at serial concentrations for 72 h of normal incubation relative to the untreated control group. The mortality profile followed a dose-related response. The activity was more intense at higher concentrations ($P < 0.001$) (Fig. 5).

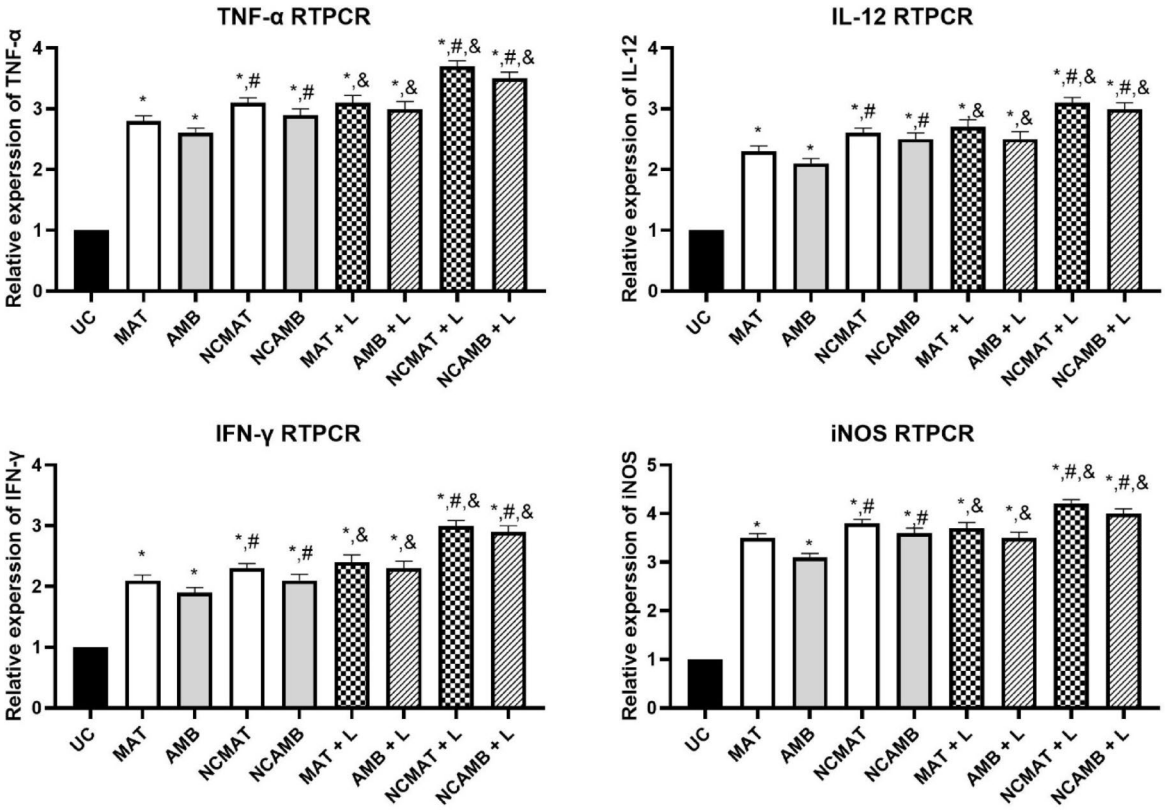

Fig. 4. M1 macrophage-related gene expression cytokines of MAT, AMB, NCMAT, and NCAMB with and without light compared to the control group. Bars are standard deviation (*$P < 0.001$ with UC), (#$P < 0.001$ MAT or AMB vs. NC form), (& <0.001 with vs. without light).

Anti-amastigote assessment

Various concentrations of MAT, AMB, NCMAT, and NCAMB with and without light caused a significant decrease in the overall number of intra-macrophage amastigotes (clinical stage) rather than the untreated control groups ($P < 0.001$) (Table 3).

Cytotoxic effects and combination index

Different concentrations of MAT and NCMAT with and without light were studied on the macrophage cell line (Table 4).

M1 and M2 type cytokines

The expression of the selected gene profile linked with M1 macrophage cytokines is presented in Fig. 4. In Fig. 6 the changes of M1 macrophage cytokines are presented. The M2 macrophage cytokines are presented in Fig. 7. The results show a significant decrease in M2-related macrophages and a significant increase in M1 macrophages-related cytokines.

Apoptotic profiles

Cell cycle arrest

The result of the cell cycle assay showed in treatment groups compared to the control group. Induction at the sub-G0/G1 phase significantly arrested the cell cycle phases (Fig. 8).

ROS production

The result of the ROS production assay showed in treatment groups compared to the control group. (Fig. 9).

Discussion

The current study aimed to evaluate the potential of Co-Fe_2O_4@GO-poly (AMPS-co-AM) nanocomposites as nanocarriers for the delivery of MAT and AMB in the treatment of *L. tropica*. This novel nanocomposite was designed to enhance the delivery of MAT and AMB, the widely used anti-leishmanial drugs. The significant findings of this study suggest that these nanocomposites not only improve drug delivery but also enhance the efficacy and safety of PDT. This approach has demonstrated notable anti-leishmanial effects in both the promastigote and amastigote stages of *L. tropica*. The ability of nanomaterials to serve as efficient drug delivery systems, particularly in the realm of neglected tropical diseases (NTDs) like leishmaniasis, holds great promise.

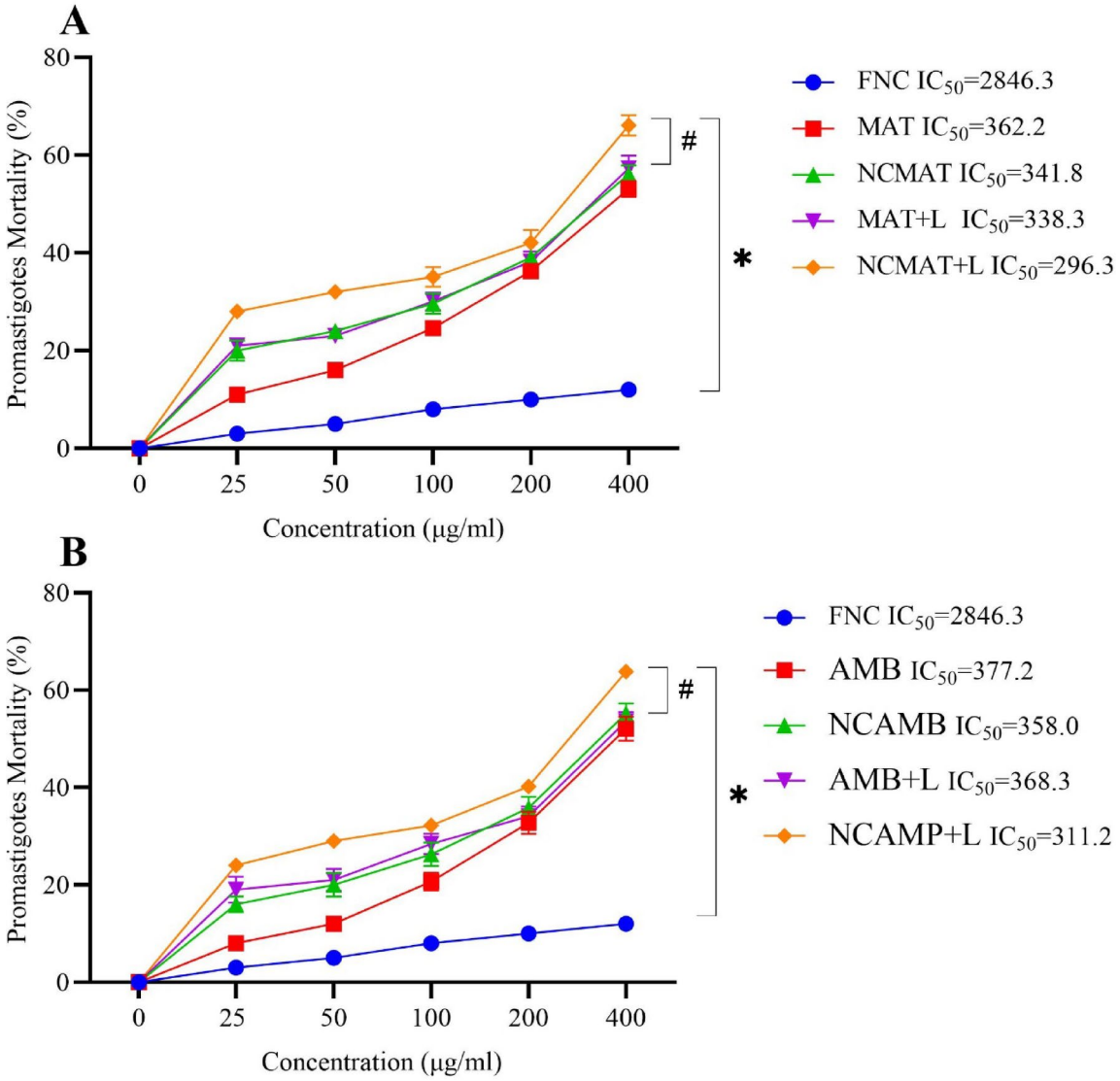

Fig. 5. The values of total mean mortality in promastigotes of *L. tropica* parasite at different concentrations of MAT, AMB, NCMAT, and NCAMB with and without light, and the light-only control (Light only). *Significant difference in comparison to the untreated control group (UC) (*$P < 0.001$) #Significant difference between with vs. without light ($P < 0.05$).

This study builds upon the growing body of evidence that suggests nanotechnology can revolutionize the treatment of parasitic infections by improving drug efficacy, minimizing side effects, and facilitating the targeting of intracellular pathogens[46–49].

MAT is well-established in the treatment of leishmaniasis, but its therapeutic potential is often limited by issues such as drug resistance, toxicity, and side effects[50,51] AMB is considered a second-line treatment for CL, but its use is restricted due to its high cost and nephrotoxicity[52] In this study, the nanocomposites demonstrated the ability to carry a high payload of MAT and AMB, as confirmed by the UV spectrophotometer analysis. The loading capacity of MAT (0.196 g per gram of nanocomposite) and AMB (0.178 g per gram of nanocomposite) suggests that these nanocarriers can hold significant amounts of the drugs, ensuring sustained and targeted release. The magnetic properties of the Co-Fe_2O_4 core allow for targeted drug delivery, particularly when used in conjunction with an external magnetic field, potentially reducing the off-target effects and enhancing the drug's efficacy at the injection site.

The in vitro results showed a significant reduction in both promastigote and amastigote viability when treated with NCMAT or NCAMB, both with and without light activation, compared to the forms without nanocomposite and the untreated control group. The combination of the nanocomposites with PDT (NCMAT + L and NCAMB + L) yielded the highest level of efficacy, indicating the synergistic potential of combining drug-loaded nanocomposites with light activation to enhance leishmanicidal activity. NCAMB + L demonstrated efficacy comparable to NCMAT + L, further supporting the versatility of the Co-Fe_2O_4@GO-poly (AMPS-co-AM) platform.

Concentration (µg/ml)	FNC		MAT		AMB		NCMAT		NCAMB		MAT + L		AMB + L		NCMAT + L		NCAMB + L	
	Mean ± SD	*P* value	Mean ± SD	*P* value	Mean ± SD	*P* value	Mean ± SD	*P* value	Mean ± SD	*P* value	Mean ± SD	*P* value	Mean ± SD	*P* value	Mean ± SD	*P* value	Mean ± SD	*P* value
0 (UC)	69.4 ± 0.8	NR	69.4 ± 0.8	NR	69.4 ± 0.8	NR	69.4 ± 0.8	NR	69.4 ± 0.8	NR	69.4 ± 0.8	NR	69.4 ± 0.8	NR	69.4 ± 0.8	NR	69.4 ± 0.8	NR
25	65.1 ± 0.6	0.37	48.1 ± 1.2	< 0.001	50.1 ± 1.5	< 0.001	44.6 ± 0.8	< 0.001	46.1 ± 1.1	< 0.001	48.5 ± 1.2	< 0.001	50.3 ± 1.3	< 0.001	40.4 ± 1.3	< 0.001	45.1 ± 1.2	< 0.001
50	62.1 ± 1.0	0.86	40.6 ± 0.9	< 0.001	45.1 ± 1.4	< 0.001	37. 2 ± 0.7	< 0.001	31.3 ± 0.7	< 0.001	39.2 ± 0.6	< 0.001	40.1 ± 0.8	< 0.001	36.1 ± 0.7	< 0.001	38.2 ± 0.8	< 0.001
100	58.9 ± 0.9	0.31	35.1 ± 1.4	< 0.001	37.2 ± 0.9	< 0.001	23.4 ± 1.2	< 0.001	27.4 ± 0.4	< 0.001	25.3 ± 0.8	< 0.001	29.8 ± 0.9	< 0.001	12.3 ± 0.4	< 0.001	17.8 ± 0.3	< 0.001
200	52.4 ± 0.7	< 0.001	12.3 ± 0.2	< 0.001	15.3 ± 0.7	< 0.001	8.6 ± 0.2	< 0.001	10.2 ± 0.1	< 0.001	9.2 ± 0.3	< 0.001	11.7 ± 0.4	< 0.001	0.0 ± 0.0	< 0.001	0.0 ± 0.0	< 0.001
400	48.1 ± 0.8	< 0.001	0.0 ± 0.0	< 0.001	0.0 ± 0.0	< 0.001	0.0 ± 0.0	< 0.001	0.0 ± 0.0	< 0.001	0.0 ± 0.0	< 0.001	0.0 ± 0.0	< 0.001	0.0 ± 0.0	< 0.001	0.0 ± 0.0	< 0.001

Table 3. Comparison of the effect of different MAT, AMB, NCMAT, and NCAMB concentrations with and without light on the average number of intra-macrophage amastigotes compared to the untreated control group (UC).

	IC_{50} Amastigotes	*P* Value	CC_{50} Macrophages	SI
MAT	97.0	NR	718.17	7.40
FNC	486.3	*	4765.74	9.80
AMB	108.6	*	733.84	6.76
NCMAT	69.4	*,#	597.46	8.61
NCAMB	76.2	*,#	625.32	8.21
MAT + L	67.2	*,&	491.07	7.31
AMB + L	74.1	*,&	508.11	6.86
NCMAT + L	56.03	*,#,&	468.65	8.36
NCAMB + L	60.2	*,#,&	489.34	8.13

Table 4. Evaluation of IC_{50} values for MAT, AMB, NCMAT, and NCAMB with and without light against promastigotes and amastigotes of *L. tropica* compared to MA and CC_{50} values of drugs on macrophages to calculate the SI. (*$P < 0.001$ with MA), (#$P < 0.001$ MAT or AMB vs. NC form), (& <0.001 with vs. without light).

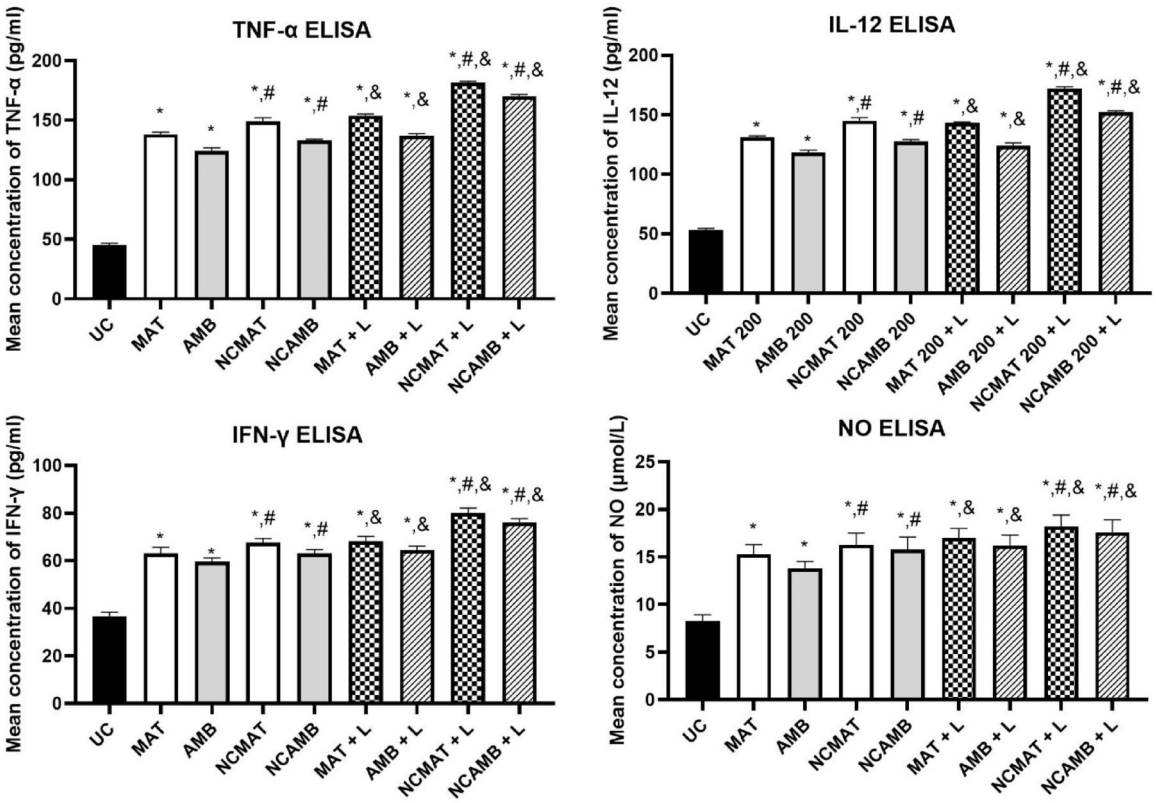

Fig. 6. M1 macrophage-related profiles cytokines of MAT, AMB, NCMAT, and NCAMB with and without light compared to the control group. Bars are standard deviation (*$P < 0.001$ with UC), (#$P < 0.001$ MAT or AMB vs. NC form), (& <0.001 with vs. without light).

In the promastigote assay, the treatment exhibited a significant dose-dependent increase in mortality. NCMAT and NCAMB outperformed MAT and AMB, respectively, as indicated by their lower IC_{50} values, demonstrating enhanced efficacy. The use of light activation further amplified the mortality rates, with NCMAT + L and NCAMB + L showing the best results, achieving the highest levels of parasite eradication compared to their counterparts without light ($P < 0.05$) and the untreated control group ($P < 0.001$) (Fig. 5). These findings underscore the potential of PDT to enhance the efficacy of nanoparticle-based treatments against *L. tropica* promastigotes.

Our study demonstrates the promising potential of nanocomposite-mediated PDT for CL treatment. To better contextualize these findings, it is important to compare this approach with existing alternative therapies. The current standard treatments for CL include pentavalent antimonials (like MAT), L-AMB, and miltefosine. Pentavalent antimonials, while widely used, suffer from increasing drug resistance and significant systemic toxicity, as highlighted in our introduction. L-AMB is more effective in many cases, especially for severe or

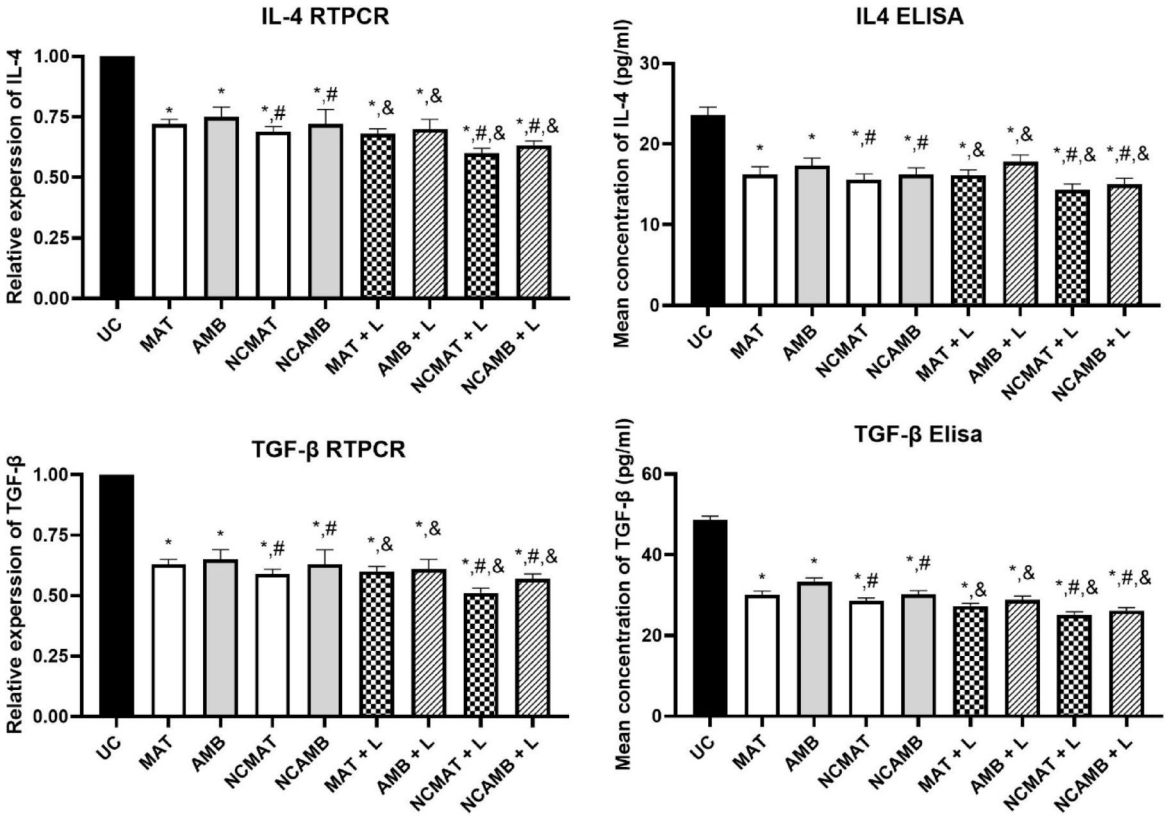

Fig. 7. M2 macrophage-related gene expression cytokines of MAT, AMB, NCMAT, and NCAMB with and without light compared to the control group. Bars are standard deviation ($^{*}P < 0.001$ with UC), ($^{\#}P < 0.001$ MAT or AMB vs. NC form), ($^{\&}$ <0.001 with vs. without light).

complicated CL, but its use is limited by nephrotoxicity and high cost[51,52]. Miltefosine, an oral drug, offers convenience but is associated with gastrointestinal side effects and teratogenicity, restricting its use in pregnant women[53]. Our nanocomposite-PDT approach offers several potential advantages. The targeted delivery of drugs using nanocomposites can enhance efficacy while minimizing systemic toxicity. PDT is a localized treatment, reducing the risk of damage to healthy tissues. Moreover, the components of our nanocomposite system offer additional benefits: the magnetic properties of Co-Fe_2O_4 allow for potential targeted delivery, and GO can be modified for improved biocompatibility. Specifically, in our study, NCMAT combined with PDT resulted in a significant reduction in parasite viability compared to MAT alone. This enhanced activity is likely attributed to increased ROS production and immunomodulation. However, nanocomposite-PDT also has limitations. It requires access to light sources and may be less effective for deep-seated lesions. Furthermore, the long-term efficacy and safety of nanocomposites need further investigation.

Similarly, the anti-amastigote assays showed that the nanocomposites were highly effective in reducing the number of intracellular amastigotes within macrophages, even at low concentrations, compared to the untreated control group ($P < 0.001$). The IC_{50} values obtained for NCMAT + L and NCAMB + L were notably lower than for free drugs, indicating that the nanocomposites significantly improve the drug's efficacy in targeting the intracellular stage of the parasite, which is the clinical stage responsible for disease pathology (Table 3). These findings are consistent with previous research that suggests the use of nanoparticles enhances the internalization of drugs by macrophages, the primary host cells for Leishmania parasites[53,54] The small size and surface modification of the nanocomposites likely contributed to their increased uptake by infected macrophages, leading to enhanced anti-leishmanial activity.

PDT has emerged as a powerful adjunctive therapy for a range of microbial infections, including leishmaniasis[20,55] It operates by inducing the generation of ROS, which leads to oxidative damage and cell death in the targeted organisms. In this study, the use of NCMAT + L and NCAMB + L, led to a significant increase in ROS production, as measured by the anthracene and methylene blue assays. ROS generation is a critical mechanism through which PDT exerts its anti-parasitic effects. The nanocomposites demonstrated excellent optical stability and maintained their ability to generate ROS even after prolonged exposure to 400 nm LED irradiation. This suggests that the nanocomposites can sustain ROS production over a prolonged period, making them highly effective for repeated PDT treatments. This observed plateau in ROS generation after 15 min warrants further discussion. We hypothesize that this plateau could be attributed to several factors within the in vitro system, including potential depletion of available dissolved oxygen required for ROS generation, possible photobleaching of the nanocomposite photosensitizer under continuous irradiation, or a saturation point in the

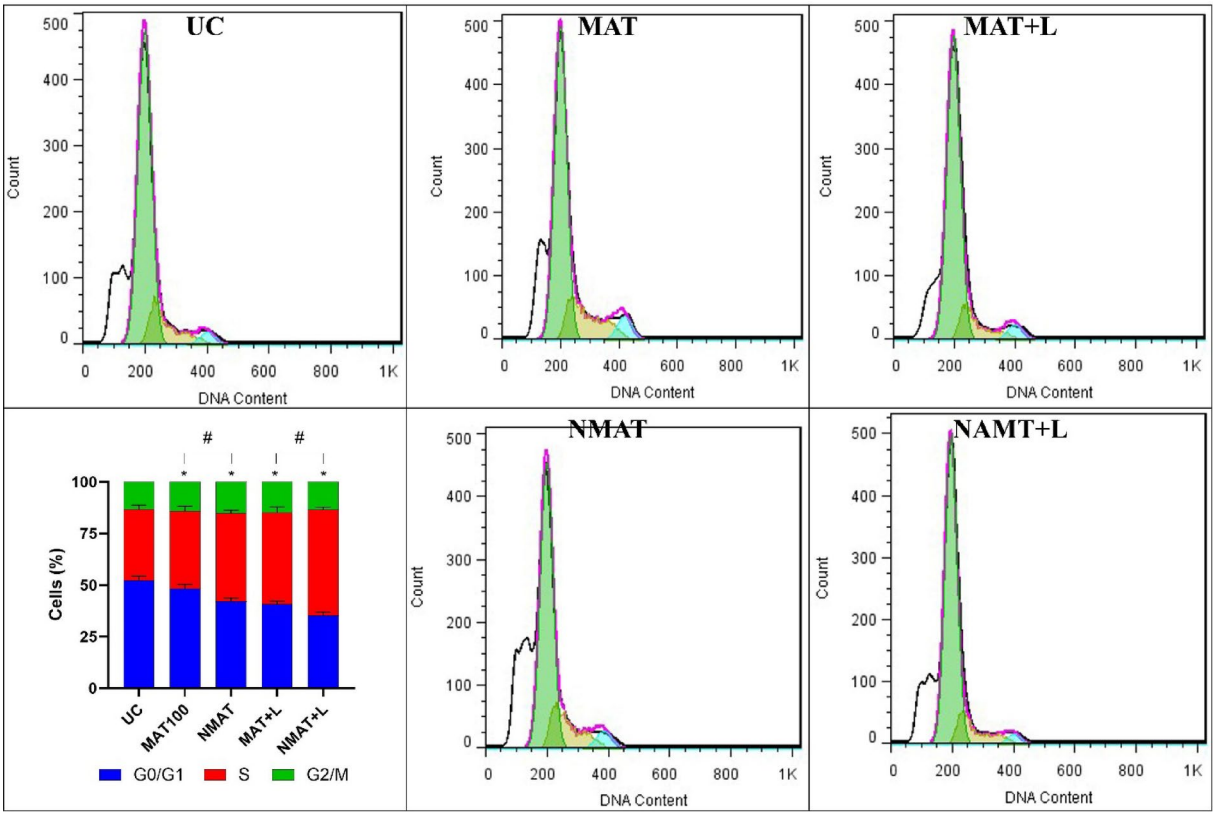

Fig. 8. Effect of MAT, AMB, NCMAT, and NCAMB with and without light compared to the control group on Leishmania tropica promastigotes cycle arrest. Bars are standard deviation (*$P < 0.001$).

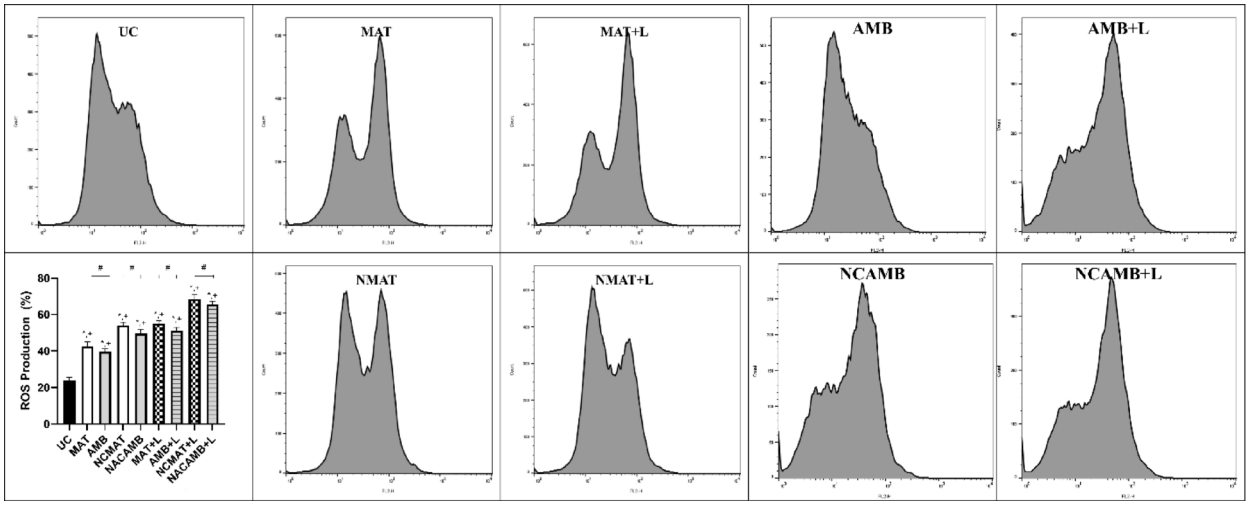

Fig. 9. Effect of MAT, AMB, NCMAT, and NCAMB with and without light in comparison to the control group on ROS production of *L. tropica* amastigotes. Bars are standard deviation (*$P < 0.001$ compared UC), (+ < 0.001 with vs. without light).

reaction kinetics between the nanocomposite and oxygen. Understanding this plateau has potential implications for clinical applications; it suggests that optimizing PDT efficacy in vivo might involve protocols using multiple, shorter light exposures rather than a single, prolonged one. This approach could potentially manage oxygen availability and minimize photobleaching effects, thereby maximizing the therapeutic outcome. Further investigation is needed to fully elucidate the precise mechanism behind the plateau and to determine optimal irradiation strategies for clinical translation. This suggests that a short burst of light exposure may be sufficient to activate the nanocomposites and achieve therapeutic efficacy. The enhanced ROS production observed in this

study aligns with previous research in the field of PDT, where nanoparticles have been shown to significantly amplify ROS generation due to their high surface area and ability to carry photosensitizers[56]. The Co-Fe_2O_4@GO-poly (AMPS-co-AM) nanocomposites used in this study not only serve as carriers for MAT and AMB but also act as efficient photosensitizers, further enhancing the therapeutic potential of PDT.

A critical consideration for any nanomaterial-based therapy is its potential toxicity and fate within the body. Nanoparticles can accumulate in various tissues, raising concerns about long-term toxicity. Therefore, it is crucial to address the biocompatibility and biodegradability of our Co-Fe_2O_4@GO-poly(AMPS-co-AM) nanocomposites. To enhance biocompatibility and reduce potential toxicity, we incorporated PEGylation into our nanocomposite design. PEGylation is a well-established method to modify nanoparticles, increasing their hydrophilicity and reducing their interaction with plasma proteins, which can minimize opsonization and clearance by the reticuloendothelial system[54]. This can prolong their circulation time and reduce off-target accumulation. In our study, the MTT assay results showed low toxicity of NCMAT and NCAMB with and without light. Furthermore, the GO component of our nanocomposites offers the potential for biodegradability. GO can be degraded by enzymes in biological systems, which is advantageous for minimizing long-term accumulation[55]. However, the degradation rate and pathways of our specific nanocomposite formulation need to be thoroughly investigated. It is important to acknowledge that while these design features aim to improve safety, comprehensive *in vivo* studies are essential to fully assess the toxicity, biodistribution, and clearance of the Co-Fe_2O_4@GO-poly(AMPS-co-AM) nanocomposites.

A key consideration in the development of any new therapeutic agent is its safety profile. The cytotoxicity assays conducted in this study revealed that NCMAT and NCAMB exhibited minimal cytotoxicity toward human macrophage cells, as evidenced by the high CC50 values (Table 4). This is a crucial finding, demonstrating the selective toxicity of the nanocomposites towards Leishmania parasites while sparing host cells. The calculated SI values for the nanocomposites further confirm their potential as safe and effective therapeutics. The particularly favorable SI values for NCMAT + L and NCAMB + L indicate that combining PDT with drug-loaded nanocomposites enhances selectivity for the parasite while minimizing host toxicity. This is a significant advantage over traditional anti-leishmanial therapies, which often suffer from low selectivity and high toxicity, leading to adverse side effects in patients. The ability of the nanocomposites to deliver drugs specifically to infected macrophages, while minimizing exposure to healthy cells, could reduce the systemic side effects associated with current treatments. This is particularly important for drugs like MAT and AMB, which are associated with significant toxicity when administered systemically[6,14,57–59].

In addition to their direct anti-leishmanial effects, the nanocomposites also demonstrated significant immunomodulatory properties. The expression of M1 and M2 macrophage-associated cytokines was assessed in this study to evaluate the impact of the nanocomposites on the host immune response. The findings demonstrated that treatment with nanocomposites led to a significant upregulation of Th1 cytokines, such as TNF-α and IFN-γ, which are associated with a pro-inflammatory immune response essential for parasite clearance ($P < 0.001$). The greatest upregulation was observed with NCMAT + L and NCAMB + L, which significantly boosted the expression of these cytokines, highlighting the pivotal role of PDT in enhancing an effective immune response against parasites compared to treatments without light activation ($P < 0.001$). Additionally, higher NO levels, an indicator of macrophage activation, support the theory that NCMAT + L and NCAMB + L stimulate a strong immune response against the parasite. The reduction of Th2 cytokines, such as IL-4 and TGF-β, further confirms that the nanocomposites regulate the immune response to enhance parasite clearance. Nanoparticles have been shown to enhance antigen presentation, activate macrophages, and stimulate the production of pro-inflammatory cytokines, all of which contribute to improved pathogen clearance. The ability of the NCMAT + L and NCAMB + L to modulate the immune response in favor of a Th1 profile suggests that they could be used not only as direct anti-leishmanial agents but also as immune adjuvants in combination with other therapies (Figs. 4, 6 and 7).

Figure 10 demonstrates that NCMAT and NCAMB are more effective in inducing apoptosis in *L. tropica* amastigotes than free drugs, as evidenced by the higher rates of programmed cell death observed in the nanocomposite-treated groups. Moreover, the addition of light activation (PDT) significantly amplified the apoptotic effect, with NCMAT + L and NCAMB + L showing the highest levels of apoptosis, far surpassing the non-light treatments and the untreated control group ($P < 0.001$).

Additionally, NCAMB + L caused significant arrest in the sub-G0/G1 phase, similar to NCMAT + L, effectively halting parasite replication ($P < 0.001$). This arrest suggests that NCMAT + L and NCAMB + L effectively interfere with the replication and survival of the parasites, further contributing to the increased apoptosis (Fig. 10).

ROS production is markedly increased in the NCMAT + L and NCAMB + L groups compared to other treatments such as NCMAT and NCAMB, reinforcing the effectiveness of PDT ($P < 0.001$). Elevated ROS levels are a known mechanism of inducing oxidative stress and cell death in parasites, and the nanocomposite forms combined with light appear to generate the highest ROS levels, which correlates with the enhanced apoptotic effects seen in these groups (Fig. 8).

The study highlights the potential of combining nanotechnology with PDT to improve leishmaniasis treatment. Co-Fe_2O_4@GO-poly (AMPS-co-AM) nanocomposites offer advantages over traditional therapies by enhancing ROS production and modulating immune responses. PDT's low toxicity and ability to target local lesions without damaging surrounding tissue make it ideal for treating localized infections common in leishmaniasis. Additionally, the affordability and portability of LED-based PDT devices are beneficial for use in resource-limited areas. Nanocomposites also present a safer alternative to traditional treatments like MAT and AMB, which have significant side effects and risks of drug resistance. They can directly target infected macrophages, reducing systemic toxicity and minimizing side effects. The magnetic properties of Co-Fe_2O_4 further enhance precision in targeting infection sites. PDT's ROS generation complements traditional therapies by inducing parasite death, potentially addressing drug resistance. Compared to costly treatments like liposomal

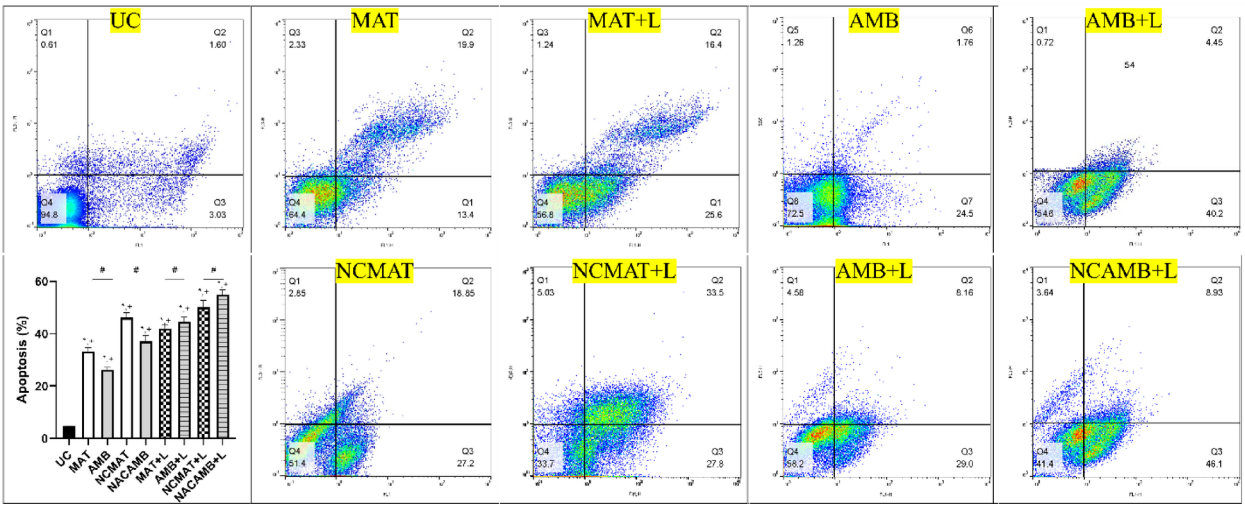

Fig. 10. Effect of MAT, AMB, NCMAT, and NCAMB with and without a light on programmed cell death of *Leishmania tropica* amastigotes compared to the untreated control group (*$P < 0.001$ compare UC), (+ < 0.001 with vs. without light).

AMB and teratogenic miltefosine, the nanocomposite-PDT approach is a more cost-effective and scalable option, especially for rural and endemic regions.

While the flow cytometry results clearly indicate an increase in apoptotic *L. tropica* promastigotes and cell cycle arrest at the sub-G0/G1 phase following treatment with NCMAT-PDT, further elucidation of the specific molecular pathways involved would strengthen these findings. We did not directly measure caspase activation in the current study. However, given that cell cycle arrest in the sub-G0/G1 phase is often associated with DNA fragmentation, a hallmark of late-stage apoptosis frequently mediated by effector caspases, we hypothesize that the observed apoptosis likely proceeds through a caspase-dependent pathway. Future studies specifically designed to investigate the activation cascade of key initiator and effector caspases would be valuable to confirm this hypothesis and provide a more detailed mechanistic understanding of NCMAT-PDT induced apoptosis in *L. tropica*.

While the results are promising, the study was limited to in vitro experiments on *L. tropica* promastigotes and amastigotes. Future studies should focus on in vivo models to better understand the interactions between the nanocomposites and the host immune system. Investigating the immune system's role in leishmaniasis progression and resolution will be critical for determining the clinical applicability of the treatment. Another area for future research is the long-term stability of the nanocomposites in biological systems. Evaluating biodegradation, clearance, and the potential for accumulation in non-target organs is essential for ensuring the safety and efficacy of the treatment.

Conclusion

This study demonstrates that combining nanotechnology with PDT presents a promising approach to leishmaniasis treatment. The Co-Fe_2O_4@GO-poly (AMPS-co-AM) nanocomposites have shown significant potential by boosting ROS production and modulating immune responses, enhancing therapeutic effectiveness against *L. tropica* in vitro. With their low toxicity, precise targeting abilities, and the accessibility of LED-based PDT devices, this method is well-suited for use in resource-limited and endemic areas. Moreover, nanocomposites present a potentially safer alternative to existing treatments. However, several challenges must be addressed before this nanocomposite-PDT approach can be translated to clinical settings. Primarily, further research is necessary to fully evaluate the safety and efficacy of this treatment in vivo. Studies in animal models are crucial to assess treatment outcomes, potential toxicity, long-term stability, and nanocomposite clearance. Additionally, regulatory hurdles associated with the development and approval of new nanomedicine-based therapies must be considered. These include demonstrating large-scale manufacturing feasibility, establishing rigorous quality control procedures, and meeting specific regulatory requirements for clinical trials and drug approval. Despite these challenges, the nanocomposite-PDT approach stands out as a cost-effective, scalable, and potentially safer alternative to existing treatments for leishmaniasis. As the burden of NTDs grows globally, innovative treatments like this will be essential in combating leishmaniasis and improving health outcomes in affected regions.

Data availability

The datasets used and analyzed during the current study are available from the corresponding author.

Received: 17 February 2025; Accepted: 2 May 2025
Published online: 10 May 2025

References

1. Aflatoonian, M. R. et al. Associated-risk determinants for anthroponotic cutaneous leishmaniasis treated with Meglumine antimoniate: A cohort study in Iran. *PLoS Negl. Trop. Dis.* **13**, e0007423 (2019).
2. Pasquier, G. et al. Leishmaniasis epidemiology in endemic areas of metropolitan France and its overseas territories from 1998 to 2020. *PLoS Negl. Trop. Dis.* **16**, e0010745. https://doi.org/10.1371/journal.pntd.0010745 (2022).
3. Khosravi, A., Sharifi, I., Dortaj, E., Afshar, A. A. & Mostafavi, M. The present status of cutaneous leishmaniasis in a recently emerged focus in south-west of Kerman Province, Iran. *Iran. J. Public. Health.* **42**, 182 (2013).
4. Roatt, B. M. et al. Recent advances and new strategies on leishmaniasis treatment. *Appl. Microbiol. Biotechnol.* **104**, 8965–8977 (2020).
5. Eskandari, S. E. et al. Combination of topical liposomal amphotericin B and glucantime in comparison with glucantime alone for the treatment of anthroponotic cutaneous leishmaniasis (ACL) caused by leishmania tropica: study protocol for a randomized, controlled trial. *Iran. J. Microbiol.* **13**, 718 (2021).
6. Albalawi, A. E. et al. Therapeutic potential of green synthesized copper nanoparticles alone or combined with meglumine antimoniate (Glucantime(®)) in cutaneous leishmaniasis. *Nanomaterials (Basel).* **11** https://doi.org/10.3390/nano11040891 (2021).
7. Khosravi, A. et al. Toxico-pathological effects of Meglumine antimoniate on human umbilical vein endothelial cells. *Toxicol. In Vitro.* **56**, 10–18 (2019).
8. Khosravi, A. et al. Vascular apoptosis associated with Meglumine antimoniate: in vivo investigation of a chick embryo model. *Biochem. Biophys. Res. Commun.* **505**, 794–800 (2018).
9. Assolini, J. P. et al. Nanomedicine in leishmaniasis: A promising tool for diagnosis, treatment and prevention of disease-An update overview. *Eur. J. Pharmacol.* **923**, 174934 (2022).
10. Assolini, J. P. et al. Nanomedicine in leishmaniasis: A promising tool for diagnosis, treatment and prevention of disease - An update overview. *Eur. J. Pharmacol.* **923**, 174934. https://doi.org/10.1016/j.ejphar.2022.174934 (2022).
11. Seyedi, F. et al. Comparison of cytotoxicity of miltefosine and its Niosomal form on chick embryo model. *Sci. Rep.* **14**, 2482 (2024).
12. Khosravi, A. et al. Cytotoxicity of amphotericin B and ambisome: in Silico and in vivo evaluation employing the chick embryo model. *Front. Pharmacol.* **13**, 860598 (2022).
13. Gonzalez, U. et al. Designing and reporting clinical trials on treatments for cutaneous leishmaniasis. *Clin. Infect. Dis.* **51**, 409–419 (2010).
14. Brito, N. C., Rabello, A. & Cota, G. F. Efficacy of pentavalent antimoniate intralesional infiltration therapy for cutaneous leishmaniasis: A systematic review. *PLoS One.* **12**, e0184777 (2017).
15. Bamorovat, M. et al. A single-group trial of end-stage patients with anthroponotic cutaneous leishmaniasis: levamisole in combination with glucantime in field and laboratory models. *Microb. Pathog.* **128**, 162–170 (2019).
16. Oliaee, R. T. et al. The potential role of nicotinamide on leishmania tropica: an assessment of inhibitory effect, cytokines gene expression and arginase profiling. *Int. Immunopharmacol.* **86**, 106704 (2020).
17. Bamorovat, M. et al. Leishmania tropica isolates from non-healed and healed patients in Iran: A molecular typing and phylogenetic analysis. *Microb. Pathog.* **116**, 124–129 (2018).
18. Bamorovat, M. et al. Host's immune response in unresponsive and responsive patients with anthroponotic cutaneous leishmaniasis treated by Meglumine antimoniate: A case-control study of Th1 and Th2 pathways. *Int. Immunopharmacol.* **69**, 321–327 (2019).
19. Tardivo, J. P., Baptista, M. S., Correa, J. A., Adami, F. & Pinhal, M. A. S. Development of the tardivo algorithm to predict amputation risk of diabetic foot. *PLoS One.* **10**, e0135707 (2015).
20. Aureliano, D. P. et al. Cell death mechanisms in leishmania amazonensis triggered by methylene blue-mediated antiparasitic photodynamic therapy. *Photodiagn. Photodyn. Ther.* **23**, 1–8. https://doi.org/10.1016/j.pdpdt.2018.05.005 (2018).
21. Van den Bergh, H. On the evolution of some endoscopic light delivery systems for photodynamic therapy. *Endoscopy.* **30**, 392–407 (1998).
22. Hopper, C., Niziol, C. & Sidhu, M. The cost-effectiveness of Foscan mediated photodynamic therapy (Foscan-PDT) compared with extensive palliative surgery and palliative chemotherapy for patients with advanced head and neck cancer in the UK. *Oral Oncol.* **40**, 372–382 (2004).
23. Hur, C., Nishioka, N. S. & Gazelle, G. S. Cost-effectiveness of photodynamic therapy for treatment of Barrett's esophagus with high grade dysplasia. *Dig. Dis. Sci.* **48**, 1273–1283 (2003).
24. Hempstead, J. et al. Low-cost photodynamic therapy devices for global health settings: characterization of battery-powered LED performance and smartphone imaging in 3D tumor models. *Sci. Rep.* **5**, 10093 (2015).
25. Henderson, B. W., Busch, T. M. & Snyder, J. W. Fluence rate as a modulator of PDT mechanisms. *Lasers Surg. Med.* **38**, 489–493 (2006).
26. Allison, R., Mota, H., Bagnato, V. S. & Sibata, C. Bio-nanotechnology and photodynamic therapy—State of the Art review. *Photodiagn. Photodyn. Ther.* **5**, 19–28 (2008).
27. Le, T. S. et al. Quick and mild isolation of intact lysosomes using magnetic–plasmonic hybrid nanoparticles. *ACS Nano.* **16**, 885–896 (2022).
28. Wang, J., Sun, J., Sun, Q. & Chen, Q. One-step hydrothermal process to prepare highly crystalline Fe3O4 nanoparticles with improved magnetic properties. *Mater. Res. Bull.* **38**, 1113–1118 (2003).
29. Van Uitert, L. d. Dc resistivity in the nickel and nickel zinc ferrite system. *J. Chem. Phys.* **23**, 1883–1887 (1955).
30. Liu, J., Cui, L. & Losic, D. Graphene and graphene oxide as new nanocarriers for drug delivery applications. *Acta Biomater.* **9**, 9243–9257 (2013).
31. Song, G. et al. Aptamer-conjugated graphene oxide-based surface assisted laser desorption ionization mass spectrometry for selective extraction and detection of Aβ1–42 in an Alzheimer's disease SH-SY5 cell model. *Front. Aging Neurosci.* **14**, 993281 (2022).
32. Zheng, P. & Wu, N. Fluorescence and sensing applications of graphene oxide and graphene quantum Dots: a review. *Chem. Asian J.* **12**, 2343–2353 (2017).
33. Kalluru, P., Vankayala, R., Chiang, C. S. & Hwang, K. C. Nano-graphene oxide-mediated in vivo fluorescence imaging and bimodal photodynamic and photothermal destruction of tumors. *Biomaterials* **95**, 1–10 (2016).
34. Fannin, P. et al. Microwave absorbent properties of nanosized Cobalt ferrite powders prepared by coprecipitation and subjected to different thermal treatments. *Mater. Design.* **32**, 1600–1604 (2011).
35. Popescu, S. A. et al. Synthesis, morphology and magnetic characterization of Zn ferrite powders. *J. Electromagn. Anal. Appl.* (2010).
36. Geim, A. K. & Novoselov, K. S. The rise of graphene. *Nat. Mater.* **6**, 183–191 (2007).
37. Banerjee, S. S., Aher, N., Patil, R. & Khandare, J. Poly (ethylene glycol)-prodrug conjugates: concept, design, and applications. *J. Drug Deliv.* **2012**, 103973 (2012).
38. Zhang, W. et al. Synergistic effect of chemo-photothermal therapy using pegylated graphene oxide. *Biomaterials* **32**, 8555–8561 (2011).
39. Boroujeni, K. P., Tohidiyan, Z., Fadavi, A., Eskandari, M. M. & Shahsanaei, H. A. Synthesis and catalytic application of Poly (2-acrylamido-2-methyl-1-propanesulfonic acid-co-acrylamide) grafted on graphene oxide. *ChemistrySelect.* **4**, 7734–7744 (2019).
40. Ribeiro, J. B. P. et al. Study of the efficacy of N-methyl glucamine antimoniate (SbV) associated with photodynamic therapy using liposomal Chloroaluminium phthalocyanine in the treatment of cutaneous leishmaniasis caused by leishmania (L.) amazonensis in C57BL6 mice. *Photodiagn. Photodyn. Ther.* **26**, 261–269 (2019).

41. Ashjari, M., Dehfuly, S., Fatehi, D., Shabani, R. & Koruji, M. Efficient functionalization of gold nanoparticles using cysteine conjugated protoporphyrin IX for singlet oxygen production in vitro. *RSC Adv.* **5**, 104621–104628 (2015).
42. Mansur, A. A., Mansur, H. S., Ramanery, F. P., Oliveira, L. C. & Souza, P. P. Green colloidal ZnS quantum Dots/chitosan nano-photocatalysts for advanced oxidation processes: study of the photodegradation of organic dye pollutants. *Appl. Catal. B.* **158**, 269–279 (2014).
43. Oliveira, L. et al. A new catalyst material based on niobia/iron oxide composite on the oxidation of organic contaminants in water via heterogeneous Fenton mechanisms. *Appl. Catal. A.* **316**, 117–124 (2007).
44. Keyhani, A. et al. In vitro and in vivo therapeutic potentials of 6-gingerol in combination with amphotericin B for treatment of leishmania major infection: powerful synergistic and multifunctional effects. *Int. Immunopharmacol.* **101**, 108274 (2021).
45. Folkes, L. K. & Wardman, P. Enhancing the efficacy of photodynamic cancer therapy by radicals from plant auxin (indole-3-acetic acid). *Cancer Res.* **63**, 776–779 (2003).
46. Goonoo, N. et al. Nanomedicine-based strategies to improve treatment of cutaneous leishmaniasis. *R. Soc. Open. Sci.* **9**, 220058 (2022).
47. Torabi, N. et al. Nanogold for the treatment of zoonotic cutaneous leishmaniasis caused by leishmania major (MRHO/IR/75/ER): an animal trial with methanol extract of *Eucalyptus camaldulensis*. *JPHS* **1**, 13–16 (2011).
48. Mohebali, M. et al. Nanosilver in the treatment of localized cutaneous leishmaniasis caused by leishmania major (MRHO/IR/75/ER): an in vitro and in vivo study. (2009).
49. Mohtasebi, S. et al. In vitro and in vivo anti-parasitic activity of biogenic antimony sulfide nanoparticles on leishmania major (MRHO/IR/75/ER). *Parasitol. Res.* **118**, 2669–2678 (2019).
50. Bastos, M. M., Hoelz, B., Boechat, L. V., de Oliveira, A. P. & N. & Antileishmanial chemotherapy: A literature review. *Revista Virtual De Química*. **8**, 2072–2104 (2016).
51. Franco, A. M. et al. Nanoscaled hydrated antimony (V) oxide as a new approach to first-line antileishmanial drugs. *Int. J. Nanomed.* 6771–6780 (2016).
52. Lemke, A., Kiderlen, A. & Kayser, O. Amphotericin B. *Appl. Microbiol. Biotechnol.* **68**, 151–162 (2005).
53. Nafari, A. et al. Nanoparticles: new agents toward treatment of leishmaniasis. *Parasite Epidemiol. Control.* **10**, e00156. https://doi.org/10.1016/j.parepi.2020.e00156 (2020).
54. Bruni, N. et al. Nanostructured delivery systems with improved leishmanicidal activity: a critical review. *Int. J. Nanomed.* 5289–5311 (2017).
55. Gardlo, K. et al. Treatment of cutaneous leishmaniasis by photodynamic therapy. *J. Am. Acad. Dermatol.* **48**, 893–896. https://doi.org/10.1067/mjd.2003.218 (2003).
56. Henderson, B. W. & Dougherty, T. J. How does photodynamic therapy work? *Photochem. Photobiol.* **55**, 145–157 (1992).
57. Faris, R., Jarallah, J., Khoja, T. & Al-Yamani, M. Intralesional treatment of cutaneous leishmaniasis with sodium stibogluconate antimony. *Pediatrics* **95**, 882–882 (1995).
58. Khamesipour, A. Therapeutic vaccines for leishmaniasis. *Expert Opin. Biol. Ther.* **14**, 1641–1649 (2014).
59. Khatami, A., Firooz, A., Gorouhi, F. & Dowlati, Y. Treatment of acute old world cutaneous leishmaniasis: a systematic review of the randomized controlled trials. *J. Am. Acad. Dermatol.* **57**, 335 (2007). e331-335. e329.

Acknowledgements

The authors want to thank the Leishmaniasis Research Center employees for their assistance in conductingthis study.

The authors want to thank the Leishmaniasis Research Center employees for their assistance in conducting. this study.

Author contributions

E.M., E.S., A.K., M.Z. and F.S. (methodologist and collected the data), E.S. and M.B. (analysis data and validation), A.Kh. and E.M. (original draft preparation, supervision), I.S. (review and editing). All authors read and approved the final paper.

Funding

This project was supported by the Kerman University of Medical Sciences, Kerman, Iran (Grant no. 99000897).

Declarations

Competing interests

The authors declare no competing interests.

Ethical standards

The present study was approved by the Ethics Committee of Kerman University of Medical Sciences, Kerman, Iran (Approval ID. IR.KMU.REC.1400.071).

Additional information

Correspondence and requests for materials should be addressed to A.K.